

Enhancement of the Plasma Potential by Fluctuating Electric Fields near the Ion Cyclotron Frequency

N. Hershkowitz, B. A. Nelson, J. Johnson, J. R. Ferron, H. Persing, C. Chan, S. N. Golovato,
and J. D. Callen

Nuclear Engineering Department, University of Wisconsin, Madison, Wisconsin 53706

and

J. Woo

InterScience, Inc., Troy, New York 12180

(Received 12 March 1985)

It is found that ion cyclotron resonance frequency can create an ion-plugging plasma potential equal to several times T_e/e ($\approx T_i/e$) in the Phaedrus tandem mirror end cells or at the end of the central cell. A model based on a local balance of electron expulsion by the rf field \tilde{E}_z and trapping by Coulomb scattering predicts the magnitude and scaling of the potential with density and rf antenna current. This model is in reasonable agreement with experimental observations. This ion-cyclotron resonance-frequency enhanced potential increases as the plasma density decreases and as the antenna current increases.

PACS numbers: 52.55.Mg, 52.40.Db

A key component of the tandem mirror concept¹ is ion confinement by electrostatic potential plugs at each end of a central mirror plasma. Several techniques have been used to create the plugging potentials. In the original concept neutral-beam fueling was used to create end cells with high density relative to the central cell. The plugging potential then resulted from the Boltzmann relation, $n/n_0 = \exp(e\Delta\phi/T_e)$, where $\Delta\phi$ is the plasma potential difference between points with density n and n_0 , e is the electron charge, and T_e is the electron temperature. This technique has been successfully demonstrated^{2,3} but has the disadvantage that the plug potential only depends logarithmically on density, so that large plug density is required. For example, in the TMX experiment² an ion-confining potential equal to $1.9T_e$ resulted from an end-cell to central-cell density ratio of 6.8. The need for high end-cell density was circumvented by the invention of the thermal barrier,⁴ a potential dip at each end of the central cell which allows the electron temperature in the plugs to be much higher than in the central cell. In the TMX-U experiment,⁵ thermal-barrier potential dips were achieved by a combination of neutral-beam injection and electron-cyclotron-resonance heating. It was demonstrated that significant ion-confining potentials could be achieved with plug and central-cell densities approximately equal. Similar results were also achieved in Gamma-10.⁶

In this Letter we present a new technique based on experiments in the Phaedrus tandem mirror which makes use of rf near the ion cyclotron resonance frequency (ICRF) to produce plugging potentials that are much larger than would be predicted by the Boltzmann relation. We show that the ICRF-enhanced potential is largest at low end-cell plasma density (comparable to or lower than the central-cell density), does not require neutral-beam injection or electron-cyclotron

heating, and is associated with non-Maxwellian electrons. The plugging potential peak is located on the high-magnetic-field side of the end-cell ion cyclotron resonance that is closest to the end-cell antenna, rather than at the end-cell midplane. Preliminary Phaedrus data have been reported previously,^{7,8} and some evidence for ion plugging by an rf-enhanced potential in the TARA tandem mirror has recently been reported.⁹

Our model for the rf-enhanced potential peak in the end cell assumes that a steady-state potential "well" for electrons is centered about a local peak in the component of the ICRF electric field (\tilde{E}_z) parallel to the magnetic field. This model results from computer-code calculations¹⁰ of the frequency dependence of \tilde{E}_z for Phaedrus end-cell parameters. The code assumes a uniform magnetic field. Codes for calculating \tilde{E}_z for a nonuniform magnetic field do not exist, and so we can at best obtain only a qualitative dependence of \tilde{E}_z on ω/ω_{ci} , where ω_{ci} is the ion cyclotron frequency and ω is the rf frequency. The code indicates that \tilde{E}_z is a maximum for $\omega = 0.9\omega_{ci}$. In addition the code predicts that there is a sharp peak in \tilde{E}_z in the near-field region (within 10 cm of the antenna). Thus, a localized peak in \tilde{E}_z can be expected on the end-cell magnetic field gradient in the near-field region close to the location where $\omega = 0.9\omega_{ci}$. A fraction of the electrons trapped in the well by a combination of dc electric and magnetic fields are given sufficient energy by the rf field \tilde{E}_z to be expelled during each rf cycle. In equilibrium this ICRF electron pumping rate is balanced by Coulomb scattering into the well. As the density is increased, the trapping rate increases, filling the well faster than the rf can pump it out, so that the well depth decreases (i.e., the ion-plugging potential is reduced). At lower densities the well depth should be larger since the Coulomb trapping rate is lower. As T_e is increased, the trapping rate decreases, so that the well depth in-

creases. Note that this mechanism for rf-enhanced potential formation does not depend on the electron bounce frequency as does a model previously proposed.¹¹

An estimate of the pumping rate in Phaedrus can be made by integration of the electron guiding-center equations. The electrons are launched from the midplane of the potential well, and by variation of the initial kinetic energy and pitch angle, velocity space is divided into "lost" and "trapped" regions. The pumping rate is computed by integration of the distribution function over the portion of the lost region of velocity space which is trapped in the absence of the ICRF electric field. The net in-scattering rate can be estimated from Eq. (28) in Cohen *et al.*¹² which is derived by the balancing of particle exchange across a loss cone boundary. The "steady state" plugging potential is found by balancing of the ICRF pumping rate with the rate at which electrons are scattered into the well. Both the pumping rate and the net in-scattering rate depend on the depth of the potential well and at some well depth the rates balance.

The guiding-center equations are integrated with use of a predictor-corrector algorithm. The magnetic field of the end cells is modeled by two current loops, which provide a simple mirror geometry. The spatial dependence of the ICRF electric field magnitude is taken to be Gaussian. The plugging potential is assumed to have the same Gaussian profile. Results of this calculation for Phaedrus parameters are given in Figs. 1 and 2. Figure 1 shows that the balance of pumping and

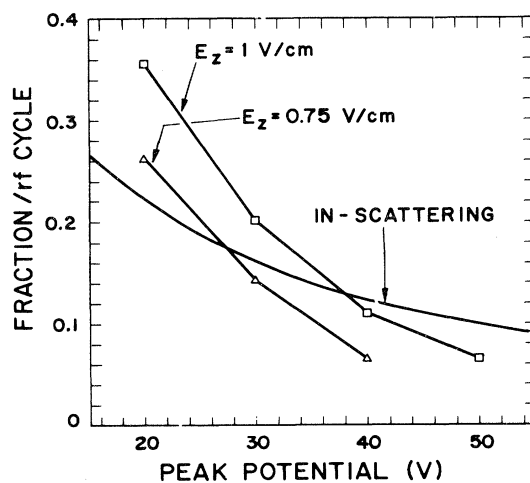


FIG. 1. Fractional change in the trapped electron density per rf cycle as a function of the peak potential. Curves are given for the pumping rates corresponding to $\tilde{E}_z = 1$ V/cm and 0.75 V/cm, and the in-scattering rate is given for trapped density $= 1 \times 10^{12}$ cm⁻³ and mirror-throat density $= 2 \times 10^{12}$ cm⁻³ and $T_e = 20$ eV. The Gaussian potential "well" is taken with a HWHM of 10 cm.

scattering for $\tilde{E}_z = 1$ V/cm is achieved when the potential peak is 37 V. The rf wave code predicts that this is approximately the value of \tilde{E}_z to expect in the near-field region of the end-cell antenna. Figure 2 shows that the model predicts that the peak confining potential should scale approximately linearly with the electron temperature.

Experiments were carried out in the rf-sustained¹³ mode of operation. In this mode both electrons and ions are heated by ICRF (at 660 kHz in the central cell and 4.3 MHz in the end cells). Line antennas 20 cm from the end-cell midplanes are used in the quadrupole end cells and a half-turn antenna 50 cm west of the central-cell midplane is operated in the central cell. The central-cell rf frequency was chosen to be approximately $0.75\omega_{ci}$. Representative plasma parameters are $n = (2-4) \times 10^{12}$ cm⁻³ and $T_e \approx 17$ eV in both the central cell and the end cells, central-cell ion temperature equal to 30 eV, and end-cell ion energy approximately equal to 1 keV. Magnetohydrodynamic stability is provided by high plasma pressure in the quadrupole end cells.¹⁴ Plug plasma potentials were directly measured with small (shaft diameters ≈ 0.08 cm), relatively nonperturbing self-emissive probes¹⁵ and indirectly by nonperturbing ion end-loss energy analyzers. Central-cell plasma potentials were measured by swept electrostatic probes and by emissive probes, and inferred from probe floating potentials.

Local measurements with self-emissive probes show that ICRF applied with inboard antennas (located on the central-cell side of the end-cell midplane) results in ion-plugging plasma potentials. Peak plasma potentials as large as 40 V greater than the central-cell plasma potential have been achieved. Representative data are given in Fig. 3(a). Note that the plasma potential peak occurs on the high-magnetic-field side of the

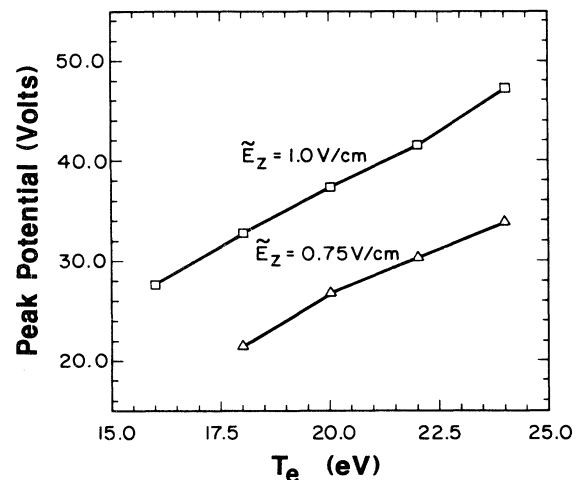


FIG. 2. Computer-code calculations of equilibrium potential vs T_e for two values of \tilde{E}_z .

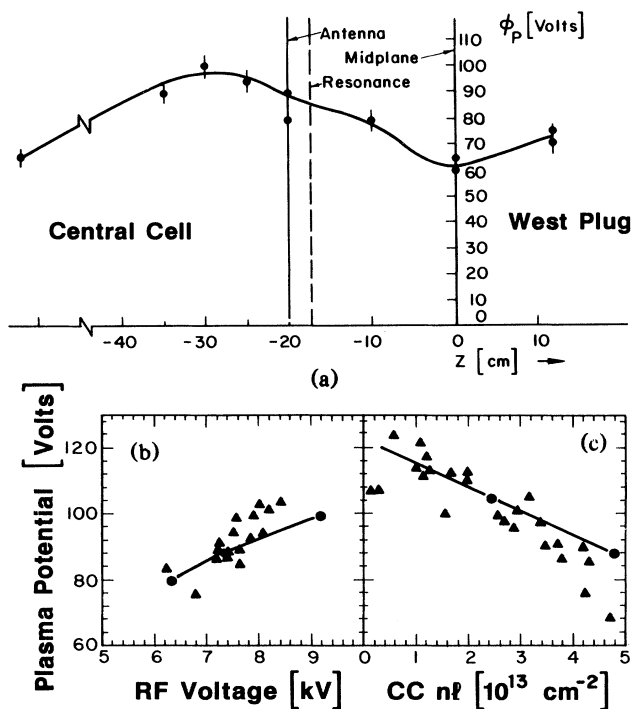


FIG. 3. Plasma potential variations in the Phaedrus tandem mirror. (a) West plug axial potential profile. The antenna is indicated by a solid vertical line and the nearby ω_{ci} resonance by a dashed vertical line. (b) Maximum west inboard plasma potential vs rf voltage applied to the west inboard antenna for fixed central-cell density. (c) Maximum west inboard potential vs central-cell line density for fixed rf voltage. Solid lines in (b) and (c) are the predictions of the model.

ICRF resonance at the location where $\omega \approx 0.9\omega_{ci}$. A significant potential peak has only been found near the resonance closest to the antenna, indicating the importance of the large \tilde{E}_z in the near-field region. End-loss ion-energy analyzer data confirm the peak plasma potentials (though not the axial location) and also show that ion end-loss currents are reduced by the plugging potential. The plasma potential at the end-cell midplane is comparable to the central-cell potential and only slight increases in potential (~ 10 V) are found near the outboard resonance.

End-cell midplane microwave interferometer and neutral-beam attenuation measurements of the end-cell axial density profile indicate that the peak end-cell density (located near the ion cyclotron resonance) is less than 1.5 times the central-cell density. The assumption of Boltzmann electrons with $T_e = 17$ eV gives a maximum end-cell to central-cell potential difference of 7 V. This is much less than the measured potential difference of up to 40 V.

Figures 3(b) and 3(c) give a comparison between the predictions of the model and the experimentally

observed dependence of the peak on axis end-cell potential, on the rf field amplitude, and on the plasma density. In Fig. 3(b) the potential is shown as a function of the voltage across the end-cell antenna (which is proportional to the antenna current) for a fixed central-cell density ($n_c = 2 \times 10^{12} \text{ cm}^{-3}$). The increase in plugging potential is approximately linear with the antenna voltage, which is proportional to the strength of the field \tilde{E}_z . The solid line gives the prediction of the model on the assumption that $\tilde{E}_z = (\text{antenna kilovoltage}) / (9.3 \text{ cm})$. Figure 3(c) shows that the end-cell potential decreases as the central-cell density increases for fixed antenna voltage (7 kV). The relevant density is the central-cell density which is proportional to the central-cell loss stream. The solid curve is the prediction of the model on the assumption that $\tilde{E}_z = 0.75$ V/cm.

It has not been possible to measure the field \tilde{E}_z experimentally, and so estimates have been obtained from McVey's code¹⁰ which analyzes wave propagation in a cylindrically symmetric plasma column with arbitrary radial density and temperature profiles and realistic antennas. We have approximated the line antennas and elliptical plasma in Phaedrus by considering a half-turn antenna, radius 10.5 cm, located concentric with a Gaussian profile plasma, with radius equal to 5.5 cm and peak density equal to $2.3 \times 10^{12} \text{ cm}^{-3}$, $B = 2.6$ kG, antenna current equal to 1000 A, and T_e and T_i equal to 20 eV and 800 eV, respectively. The code predicts that the peak field \tilde{E}_z is located 8 cm axially from the antenna and is 0.3 V/cm at $r = 0$ cm and 1.0 V/cm at $r = 6$ cm.

Ion end-loss measurements indicate that an rf-enhanced potential peak may also be formed in the central cell when conditions are similar to those described for the end cells. This result was obtained in the rf-stabilized mode of operation¹⁶ with no end-cell rf and the central-cell resonance near the central-cell midplane. The central-cell heating antenna was west of the midplane near the mirror-throat magnetic field gradient. We expect localized peaks in \tilde{E}_z on the magnetic field gradient where $\omega \approx 0.8\omega_{ci}$ (the code prediction of the frequency for peak \tilde{E}_z using central-cell parameters) at each end of the central cell. We also expect the strongest field \tilde{E}_z to be at the west end in the near-field region of the antenna. The presence of an ICRF-enhanced potential peak at the west end is indicated by total ion end-loss current to the west end which is as small as $\frac{1}{7}$ of the current to the east end (Fig. 4). When the rf is turned off, the currents immediately equalize. Swept ion end-loss energy-analyzer measurements show that the minimum energy of ions lost to the west end is larger than the minimum energy of ions lost to the east end by 5–50 V, depending on radius. The minimum energy gives the largest potential through which the ions pass. This confirms the presence of the potential peak at the west

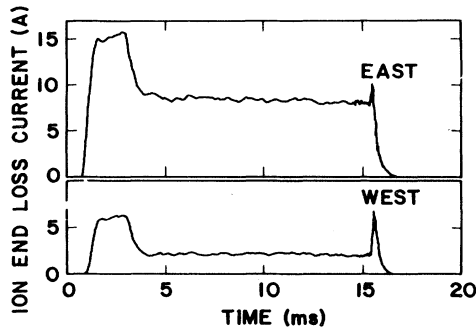


FIG. 4. Ion-loss current to the west and east walls during the rf-stabilized mode of operation. The region of measurement includes approximately one half of the flux tube which maps to the central-cell plasma. The time period 0 to 3 ms covers the plasma startup phase which results in enhanced end-loss current to both ends.

end. When the magnetic field gradient near the antenna is reduced so that the location where $\omega \approx 0.8\omega_{ci}$ moves away from the near-field region of the antenna, significant west-end plugging is not observed.

End plugging at the west end of the central cell could also be due to a ponderomotive pseudopotential,^{17,18}

$$\phi = \frac{e}{4M_i\omega} \left(\frac{E_+^2}{\omega - \omega_{ci}} + \frac{E_-^2}{\omega + \omega_{ci}} - \frac{\tilde{E}_z}{\omega} \right), \quad (1)$$

located in the near-field region of the antenna. Here E_+ and E_- are the components of the rf electric field rotating with the ions and electrons, respectively. In the end cells E_+ and E_- are comparable to central-cell values, but ω is 6 times greater, so that the pseudopotentials should be even smaller.

The maximum values of the central-cell rf electric field, as predicted by the code for the experimental parameters, are $E_+ = 4.5$ V/cm and $E_- = 23$ V/cm. For $f = 0.8f_{ci} = 660$ kHz, the total pseudopotential is only 2.2 V. This is too small to account for the end-plugging potential measured with the swept ion end-loss energy analyzer.

In summary, it has been shown that ICRF can be used to create ion-plugging plasma potentials. We be-

lieve that the potential formation depends on the balance of Coulomb scattering and electron expulsion by the ICRF field \tilde{E}_z in a localized region and that it favors low plasma density. In the Phaedrus tandem mirror this technique is the principal source of axial ion confinement. We would like to suggest that this technique might provide a useful supplement to the axial ion confinement in other tandem mirror devices. For example, an ICRF-enhanced potential produced at each end of the central cell might be used to prevent cold central-cell ions from filling the thermal barriers in TMX-U.

This work was supported by the U.S. Department of Energy under Contract No. DE-AC02-78ET51015.

¹G. I. Dimov, V. V. Zakaidakov, and M. E. Kishinevskii, *Fiz. Plazmy* **2**, 597 (1976) [*Sov. J. Plasma Phys.* **2**, 326 (1976)]; T. K. Fowler and B. G. Logan, *Comments Plasma Phys. Controlled Fusion* **2**, 167 (1977).

²F. H. Coengen *et al.*, *Phys. Rev. Lett.* **44**, 1132 (1980).

³K. Yatsu *et al.*, *Phys. Rev. Lett.* **43**, 626 (1979).

⁴D. E. Baldwin and B. G. Logan, *Phys. Rev. Lett.* **43**, 1318 (1979).

⁵D. Grubb *et al.*, *Phys. Rev. Lett.* **53**, 783 (1984).

⁶T. Cho *et al.*, in *Plasma Physics and Controlled Nuclear Fusion Research, London, 1984* (International Atomic Energy Agency, Vienna, 1985), Vol. 2, p. 275.

⁷B. A. Nelson *et al.*, *Bull. Am. Phys. Soc.* **28**, 1203 (1983).

⁸B. A. Nelson *et al.*, *Bull. Am. Phys. Soc.* **29**, 1423 (1984).

⁹D. K. Smith *et al.*, *Bull. Am. Phys. Soc.* **29**, 1267 (1984).

¹⁰B. McVey, MIT Report No. PFC/RR-84-12 and U.S. Department of Energy Report No. E DOE/ET/51013-129, 1984 (to be published).

¹¹D. K. Smith *et al.*, *Bull. Am. Phys. Soc.* **28**, 1182 (1983).

¹²R. H. Cohen, I. B. Bernstein, J. J. Dorning, and G. Rowlands, *Nucl. Fusion* **20**, 1421 (1980).

¹³R. A. Breun *et al.*, *Phys. Rev. Lett.* **47**, 1833 (1981).

¹⁴A. W. Molvik *et al.*, *Phys. Rev. Lett.* **48**, 742 (1981).

¹⁵N. Hershkowitz *et al.*, *Rev. Sci. Instrum.* **54**, 29 (1983).

¹⁶J. R. Ferron *et al.*, *Phys. Rev. Lett.* **51**, 1955 (1983).

¹⁷H. Motz and C. J. Watson, in *Advances in Electronics and Electron Physics* (Academic, New York, 1967), Vol. 23, p. 153.

¹⁸S. Okamura *et al.*, in *Plasma Physics and Controlled Nuclear Fusion Research, London, 1984* (International Atomic Energy Agency, Vienna, 1985), Vol. 2.